J Fluoresc (2014) 24:1545–1552
DOI 10.1007/s10895-014-1443-7

ORIGINAL PAPER

Deep-Red Phosphorescent Iridium(III) Complexes Containing 1-(Benzo[b] Thiophen-2-yl) Isoquinoline Ligand: Synthesis, Photophysical and Electrochemical Properties and DFT Calculations

Gao-Nan Li · Ying Zou · Yi-Ding Yang · Jiao Liang · Feng Cui · Tao Zheng · Hui Xie · Zhi-Gang Niu

Received: 7 June 2014 / Accepted: 20 August 2014 / Published online: 31 August 2014

Abstract Four new bis-cyclometalated iridium(III) complexes, [Ir(btq) $_2$phen] [PF_6] (3a), [Ir(btq) $_2$bpy] [PF_6] (3b), [Ir(btq) $_2$dtbipy] [PF_6] (3c) and [Ir(btq) $_2$pic] (3d) (btq= 1-(benzo[b] thiophen-2-yl) isoquinoline, phen=1,10-phenanthroline, bpy=2,2′-bipyridine, dtbipy=4,4′-di-tert-butyl-2,2′-bipyridine, pic=picolinic acid) have been synthesized and fully characterized. The crystal structure of 3a has been determined by X-ray analysis. The photophysical and electrochemical properties of these new complexes 3a−3d have been studied. The photoluminescence spectra of all Ir(III) complexes exhibit deep-red emission maxima at 682, 682, 683 and 698 nm, respectively. The most representative molecular orbital energy-level diagrams and the lowest energy electronic transitions of 3a−3d have been calculated with density functional theory (DFT) and time-dependent DFT (TD−DFT). The results show that the pic ancillary ligand of complex 3d influences the absorption and emission energies with a further red-shift relative to other three complexes 3a−3c.

Keywords Iridium(III) complex · Photoluminescence · Deep-red phosphorescence · Cyclic voltammetry · DFT calculation

G.-N. Li · Y. Zou · Y.-D. Yang · J. Liang · F. Cui · T. Zheng · H. Xie · Z.-G. Niu (✉)
College of Chemistry and Chemical Engineering,
Hainan Normal University, Haikou 571158, China
e-mail: niuzhigang1982@126.com

G.-N. Li
State Key Laboratory of Coordination Chemistry,
School of Chemistry and Chemical Engineering, Nanjing University,
Nanjing 210093, China

Introduction

Recently, extensive research efforts have been made for gaining more achievements in white organic light-emitting diodes (WOLEDs) as they can be used for flat panel displays and the next generation solid-state lighting sources [1–5]. For the realization of white emission, it is essential to obtain high efficiency and color purity for the three primary blue, green and red emitting materials. Although many investigations about efficient pure blue and green light-emitting complexes have been reported, the search for true red emitters are more difficult because their luminescent quantum yields tend to be lower due to the smaller energy gap [6–9]. Therefore, a great amount of efforts have been devoted to the development of red-emitting materials [10–12].

In 2001, high-efficiency red phosphor, Ir(btp) $_2$(acac) (btp=2-(2-pyridyl)-benzo[b] thiophene; acac=acetylacetonate) was reported [13]. Subsequently, various btp-based iridium complexes were frequently used as red-emitting materials in OLEDs due to its moderate phosphorescence quantum yield [14–17]. More recently, Yagi and co-workers prepared the red-emitting tri-cyclometalated iridium(III) complex containing the 1-(benzo[b] thiophen-2-yl) isoquinoline (btq) ligand, which was more effective on stabilization of the LUMO [18]. In this paper, we report a series of bis-cyclometallated btq-based iridium(III) complexes with different ancillary ligands (3a−3d) (Scheme 1). Their photophysical and electrochemical properties are investigated, and the lowest-energy electronic transitions are calculated with density functional theory (DFT) and time-dependent DFT (TD−DFT).

Scheme 1 Synthetic routes of Ir(III) complexes 3a−3d

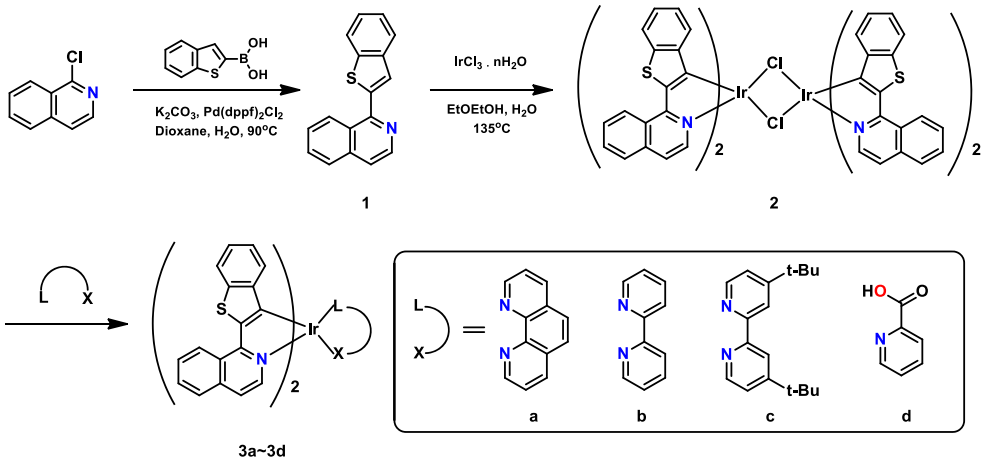

Experimental

Physical Measurements

^{1}H NMR spectra were recorded on a Bruker AM 400 MHz instrument. Chemical shifts were reported in ppm relative to Me_4Si as internal standard. FT–IR spectra were taken on a Nicolet 6700 FTIR spectrometer (400–4000 cm^{-1}) with KBr pellets. ESI−MS spectra were recorded on an Esquire HCT− Agilent 1200 LC/MS spectrometer. UV–Vis spectra were recorded on a Hitachi U3900/3900H spectrophotometer. Fluorescence spectra were carried out on a Hitachi F−7000 spectrophotometer.

The luminescence quantum efficiencies were calculated by comparison of the fluorescence intensities (integrated areas) of a standard sample *fac*-Ir(ppy) $_3$ and the unknown sample according to the equation [19–21].

$$\Phi_{unk} = \Phi_{std}\left(\frac{I_{unk}}{I_{std}}\right)\left(\frac{A_{std}}{A_{unk}}\right)\left(\frac{\eta_{unk}}{\eta_{std}}\right)^2$$

Where Φ_{unk} and Φ_{std} are the luminescence quantum yield values of the unknown sample and *fac*-Ir(ppy)$_3$ solutions (Φ_{std}=0.4) [21], respectively. I_{unk} and I_{std} are the integrated fluorescence intensities of the unknown sample and *fac*-Ir(ppy)$_3$ solutions, respectively. A_{unk} and A_{std} are the absorbance values of the unknown sample and *fac*-Ir(ppy)$_3$ solutions at their excitation wavelengths, respectively. The η_{unk} and η_{std} terms represent the refractive indices of the corresponding solvents (pure solvents were assumed).

Crystal Structure Determination

X-ray diffraction data were collected with an Agilent Technologies Gemini A Ultra diffractometer equipped with graphite-monochromated Cu Kα radiation (λ=1.54184 Å) at room temperature. Data collection and reduction were processed with CrysAlisPro software [22]. The structure was solved and refined using Full-matrix least-squares based on F^2 with program SHELXS−97 and SHELXL−97 [23] within Olex2 [24]. All non-hydrogen atoms were found in alternating difference Fourier syntheses and least-squares refinement cycles and, during the final cycles, refined anisotropically. Hydrogen atoms were placed in calculated positions and refined as riding atoms with a uniform value of *U*iso.

Electrochemical Measurements

Cyclic voltammetry (CV) was performed on a CHI 1210B electrochemical workstation, with a glassy carbon electrode as the working electrode, a platinum wire as the counter electrode, an Ag/Ag^+ electrode as the reference electrode, and 0.1 M *n*-Bu_4NClO_4 as the supporting electrolyte.

Computational Details

All calculations were carried out with Gaussian 09 software package [25]. The density functional theory (DFT) and time-dependent DFT (TDDFT) were employed with no symmetry constraints to investigate the optimized geometries and electron configurations with the Becke three-parameter Lee-Yang-Parr (B3LYP) hybrid density functional theory [26–28], with a 6-31G* basis set for C, H, O, N, and S atoms and the effective core potentials (ECP) such as LANL2DZ for Ir atoms. Solvent effects were considered within the SCRF (self-consistent reaction field) theory using the polarized continuum model (PCM) approach to model the interaction with the solvent [29, 30].

Materials

$IrCl_3 \cdot nH_2O$, 1-chloroisoquinoline and benzo[*b*]thiophen-2-ylboronic acid were purchased from Alfa Aesar. 1,10-phenanthroline, 2,2′-bipyridine, 4,4′-di-tert-butyl-2,2′-

bipyridine and picolinic acid were obtained from Energy Chemical. The target ligand, 1-(benzo[b]thiophen-2-yl)isoquinoline (**1**), was prepared according to modification of literature procedures [31]. All solvents were dried using standard procedures. Solvents used for electrochemistry and spectroscopy were spectroscopic grade.

Synthetic Procedures

*Synthesis of [Ir(btq)$_2$phen] [PF$_6$] (**3a**)*

A mixture of $IrCl_3 \cdot nH_2O$ (1.0 mmol) and the ligand **1** (2.2 mmol) in 9 mL of 2-ethoxyethanol and H_2O (v : v=2 : 1) was refluxed for 12 h. Upon cooling to room temperature, the orange precipitate was collected by filtration and washed with cooled ether and MeOH. After drying, the crude product of chloro-bridged dimer complex $[Ir(btq)_2(\mu\text{-}Cl)]_2$ (**2**) was used directly in next step without further purification. A mixture of the above dimer complex 2 (80 mg, 53.45 μmol) and 1,10-phenanthroline (24 mg, 2.5 equiv.) was dissolved in 6 mL of DCM and MeOH (v : v=1 : 1) and refluxed for 6 h under nitrogen. The orange-red solution was then cooled to room temperature, and NH_4PF_6 (44 mg, 5.0 equiv.) was added to the solution. The mixture was stirred at room temperature for 4 h, and then evaporated to dryness. The solid was purified by column chromatography with DCM / MeOH (100 : 1) eluent to afford pure product **3a** (54 mg, Yield: 56 %) as a red solid. ^{1}H NMR (400 MHz, $CDCl_3$) δ 9.08 (d, *J*=8.4 Hz, 2H), 8.65 (d, *J*=8.4 Hz, 2H), 8.20 (s, 2H), 8.18 (d, *J*=4.4 Hz, 2H), 7.74~7.86 (m, 10H), 7.17~7.22 (m, 4H), 7.10 (d, *J*= 6.8 Hz, 2H), 6.74 (t, *J*=8.0 Hz, 2H), 6.20 (d, *J*=8.4 Hz, 2H). MS-ESI: m/z 869.2 $[M-PF_6^-]^+$. IR (KBr, cm^{-1}): 2970, 2924, 2855, 1626, 1548, 1504, 1429, 1415, 1097, 843, 728, 557.

*Synthesis of [Ir(btq)$_2$bpy] [PF$_6$] (**3b**)*

Complex **3b** was obtained by the method similar to the preparation of **3a** using 2,2′-bipyridine instead of 1,10-phenanthroline (42 mg, Yield: 52 %). ^{1}H NMR (400 MHz, $CDCl_3$) δ 9.07 (d, *J*=8.0 Hz, 2H), 8.73 (d, *J*=8.4 Hz, 2H), 8.16 (t, *J*=8.0 Hz, 2H), 7.81~7.92 (m, 10H), 7.36~7.40 (m, 4H), 7.27 (d, *J*=6.8 Hz, 2H), 7.19 (t, *J*=8.0 Hz, 2H), 6.72 (t, *J*=8.0 Hz, 2H), 6.14 (d, *J*=8.4 Hz, 2H). MS-ESI: m/z 869.2 $[M-PF_6^-]^+$. IR (KBr, cm^{-1}): 2962, 2924, 2855, 1630, 1549, 1502, 1432, 1397, 1098, 845, 764, 556.

*Synthesis of [Ir(btq)$_2$dtbipy] [PF$_6$] (**3c**)*

Complex **3c** was obtained by the method similar to the preparation of **3a** using 4,4′-di-tert-butyl-2,2′-bipyridine instead of 1,10-phenanthroline (37 mg, Yield: 48 %). ^{1}H NMR (400 MHz, $CDCl_3$) δ 9.06 (d, *J*=8.0 Hz, 2H), 8.49 (s, 2H), 7.93 (d, *J*=7.6 Hz, 2H), 7.77~7.85 (m, 6H), 7.70~7.72 (m, 2H), 7.46 (d, *J*=6.4 Hz, 2H), 7.30~7.37 (m, 4H), 7.17 (t, *J*= 7.6 Hz, 2H), 6.69 (t, *J*=7.6 Hz, 2H), 6.09 (d, *J*=8.4 Hz, 2H), 1.40 (s, 18H). MS-ESI: m/z 981.4 $[M-PF_6^-]^+$. IR (KBr, cm^{-1}): 2961, 2924, 2858, 1620, 1547, 1499, 1430, 1415, 1094, 842, 734, 557.

*Synthesis of [Ir(btq)$_2$pic] (**3d**)*

A mixture of the above dimer complex **2** (80 mg, 53.45 μmol), picolinic acid (20 mg, 3.0 equiv.) and Na_2CO_3 (28 mg, 5.0 equiv.) in 2-ethoxyethanol (6 mL) was refluxed for 16 h under nitrogen. After the reaction mixture was cooled to room temperature, H_2O was added and the solid was collected by filtration. The crude product was purified by column chromatography with DCM / MeOH (100 : 1) eluent to afford pure product **3d** (45 mg, Yield: 52 %) as a red solid. ^{1}H NMR (400 MHz, $CDCl_3$) δ 9.08 (d, *J*=8.0 Hz, 1H), 9.01 (d, *J*= 8.0 Hz, 1H), 8.72 (d, *J*=6.8 Hz, 1H), 8.25 (d, *J*=7.6 Hz, 1H), 7.91 (d, *J*=8.0 Hz, 1H), 7.66~7.87 (m, 9H), 7.38 (d, *J*= 6.4 Hz, 1H), 7.27~7.32 (m, 2H), 7.13~7.19 (m, 2H), 7.06 (t, *J*=8.0 Hz, 1H), 6.78 (t, *J*=7.6 Hz, 1H), 6.62 (t, *J*=7.6 Hz, 1H), 6.49 (d, *J*=8.0 Hz, 1H), 6.08 (d, *J*=8.0 Hz, 1H). MS-ESI: m/z 836.2 $[M+1]^+$. IR (KBr, cm^{-1}): 2957, 2924, 2855, 1727, 1655, 1549, 1500, 1430, 1417, 1342, 1096, 807, 697.

Results and Discussion

Synthesis and Characterization

The required btq ligand **1** was synthesized by the suzuki reaction between 1-chloroisoquinoline and 1.2 equivalents of benzo[*b*]thiophen-2-ylboronic acid, in the presence of K_2CO_3 and $Pd(dppf)_2Cl_2$ in dioxane/water solution at 90 °C for 18 h [31]. Treatment of $IrCl_3 \cdot nH_2O$ with 2.2 equivalents of 1 in 2-ethoxyethanol/water solution at reflux gave the chloro-bridged cyclometalated iridium(III) precursor **2** which further reacted with 1,10-phenanthroline, 2,2′-bipyridine or 4,4′-di-tert-butyl-2,2′-bipyridine in the presence of NH_4PF_6 to afford cationic cyclometalated iridium(III) complexes **3a**−**3c**, respectively. Complex **3d** was obtained from the reaction of chloro-bridged dimer **2**, picolinic acid and Na_2CO_3 in 2-ethoxyethanol solution. Characterization of all these new compounds has been accomplished by FTIR, ^{1}H NMR and mass spectroscopies. In ^{1}H NMR spectra of **3a**−**3c**, the ratio of the C^N to N^N ligands is 2:1, which suggest that the chemical formula of each Ir(III) complex is $[(C^N)_2Ir(N^N)](PF_6)$. ESI mass-spectra of **3a**−**3c** exhibit a peak of the cation $[(C^N)_2Ir(N^N)]^+$, respectively. For complex **3d**, the absorptions at 1727 and 1342 cm^{-1} in the FTIR spectrum may be attributed to C=O and C−O stretching vibrations of the carboxyl groups in pic ligand.

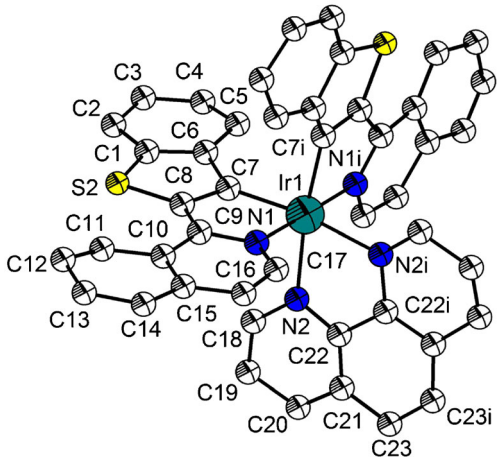

Fig. 1 ORTEP view of 3a with the thermal ellipsoids drawn at the 50 % probability level. Hydrogen atoms, solvent molecules and PF_6 anion are omitted for clarity

X-ray Crystal Structure of Complex 3a

The crystal structure of 3a was determined by X-ray diffraction analysis and the ORTEP diagram is shown in Fig. 1. The crystallographic data are listed in Table 1; selected bond lengths and bond angles are collected in Table 2.

The Ir atom in complex 3a is approximately octahedrally coordinated to two btq ligands and one phen ligand.

Table 1 Crystallographic data for complex 3a

Formula	$C_{47}H_{30}Cl_2F_6IrN_4PS_2$
M_r	1122.94
Crystal system	Monoclinic
Space group	P2/c
a (Å)	11.7493(3)
b (Å)	11.2009(2)
c (Å)	18.3649(5)
α (°)	90°
β (°)	107.421(3)°
γ (°)	90°
V (Å^3)	2306.00(10)
Z	2
ρ_c (g cm^{-3})	1.617
F(000)	1104
T / K	200.01(10)
Absorption coefficient / mm^{-1}	8.380
index ranges	−14<=h<=13 −13<=k<=12 −21<=l<=19
GOF (F^2)	1.065
R_1[a],wR_2[b]($I>2\sigma(I)$)	0.0619, 0.1629
R_1[a],wR_2[b](all data)	0.0684, 0.1733

[a] $R_1=S||F_o|-|F_c||/S|F_o|$. [b] $wR_2=[Sw(F_o^2-F_c^2)^2/Sw(F_o^2)]^{1/2}$

Table 2 Selected bond distances (Å) and angles (°) for complex 3a

Ir(1)-N(2)	2.127(6)	N(2)-C(22)	1.370(10)
Ir(1)-N(1)	2.053(6)	N(2)-C(18)	1.327(10)
Ir(1)-C(7)	2.021(7)	C(6)-C(1)	1.403(11)
S(2)-C(1)	1.733(8)	C(9)-C(8)	1.461(10)
S(2)-C(8)	1.746(7)	C(10)-C(15)	1.409(12)
N(1)-C(17)	1.374(9)	C(22)-C(22i)	1.426(16)
N(1)-C(9)	1.327(10)	C(23)-C(23i)	1.33(3)
C(12)-C(13)	1.380(16)	N(1i)-Ir(1)-N(1)	178.3(3)
N(2i)-Ir(1)-N(1i)	85.3(2)	C(7)-Ir(1)-C(7i)	90.2(4)
N(2i)-Ir(1)-N(2)	76.8(3)	C(7)-Ir(1)-N(2)	96.7(3)

Moreover, two cyclometalated btq ligands adopt *cis*-C,C' and *trans*-N,N' configuration. All Ir–C and Ir–N bond lengths are close to those in previously reported complexes [32, 33]. It is noteworthy that the Ir−N_{phen} bond length (2.127(6) Å) is slightly longer than the Ir−N_{btq} bond length (2.053(6) Å), which may be attributed to the strong *trans*-influence of the carbon donors [34]. The planar fused pyridyl ring (C9−C10−C15−C16−C17−N1) and the five-membered ring planar (C1−C6−C7−C8−S2) are almost coplanar with the relatively small dihedral angle of 1.955°.

Electronic Absorption Spectroscopy

The UV–vis absorption spectra of complexes 3a−3d in CH_2Cl_2 solution are depicted in Fig. 2, and the data are provided in Table 3. All of these complexes give almost identical absorption spectra. Intense absorption bands observed below 365 nm are attributed to the spin-allowed ligand-centered $^1\pi$-π^* transitions arising from both the cyclometalated and ancillary ligands. The weaker bands at lower energies (400–600 nm) are assigned to spin-allowed

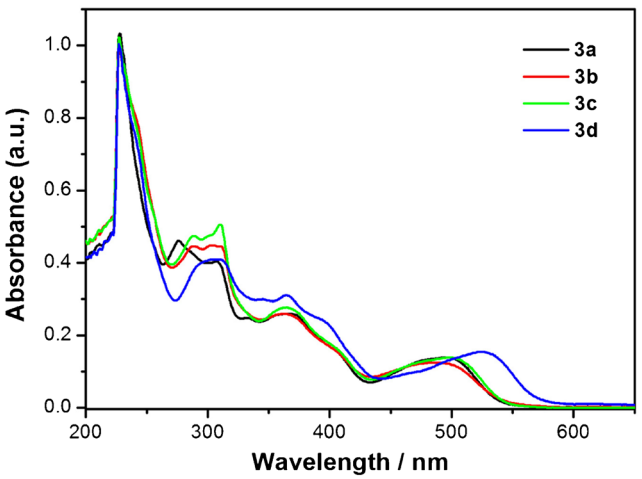

Fig. 2 Electronic absorption spectra of complexes 3a−3d in CH_2Cl_2 at room temperature

Table 3 Absorption and emission data of complexes 3a−3d

Complex	Absorption λ_{abs} / nm [a]						Emission λ_{em} (nm) [b]	Φ_{em} [b]
3a	228	276	309	365	408	500	682	0.11
3b	227	287	307	364	406	490	682	0.10
3c	227	288	310	365	407	500	683	0.12
3d	227	298	308	364	397	525	698	0.12

[a] Dichloro-methane at room temperature. [b] Degassed dichloro-methane at room temperature

singlet metal-to-ligand charge transfer (^{1}MLCT) transitions associated mainly with the btq ligand, as reported in related examples [35–38]. However, it is found that the electron-donating tert-butyl groups on the bpy ligand of complex 3c cause the absorption maximum red-shift of 10 nm in the latter low-energy region. In the cases of complex 3d, the introduction of oxygen ion on the pic ligand results in a more red-shifted absorption band than 3a−3c. The findings indicate that the electron-donating groups of the ancillary ligand could lower the energy gap between HOMO and LUMO.

Theoretical Calculations

Density functional theory (DFT) and time-dependent DFT (TDDFT) calculations were performed for complexes 3a−3d to investigate the lowest-energy electronic transition of ultraviolet absorption spectra. Molecular orbitals were calculated in dichloro-methane solution using gas-phase optimized geometries. The most representative molecular frontier orbital diagrams and the energy gap are presented in Fig. 3. The calculated spin-allowed electronic transitions and electron density distributions are summarized in Tables 4 and 5.

For all of the complexes, the electron density in HOMO is mainly dominated by iridium *d* orbitals and π–orbitals of benzothienyl groups of the cyclometalated ligands, whereas the LUMO is mainly located on the ancillary ligands. In addition, the electron density in LUMO+3 (3a), LUMO+2 (3b) and LUMO+2 (3c) predominantly localizes on the π^* orbitals of quinolinyl and benzothienyl units. The theory calculations of DFT show that the lowest-energy electronic transitions (500 nm for 3a, 490 nm for 3b, 500 nm for 3c, 525 nm for 3d) are arised from HOMO→LUMO+3 (3a), HOMO→LUMO+2 (3b), HOMO→LUMO+2 (3c) and HOMO→LUMO (3d) orbital electronic transitions, respectively (Table 4). The corresponding energy gap is 3.068 eV for 3a, 3.070 eV for 3b, 3.072 eV for 3c, and 2.938 eV for 3d (Fig. 3). In comparison with 3a−3c, the reduction of energy gap for 3d is consistent with the red shift observed along this series in absorption spectra.

Emission Properties

The normalized emission spectra of 3a−3d in degassed CH_2Cl_2 solution at room temperature are given in Fig. 4, and the corresponding data are also listed in Table 3. As

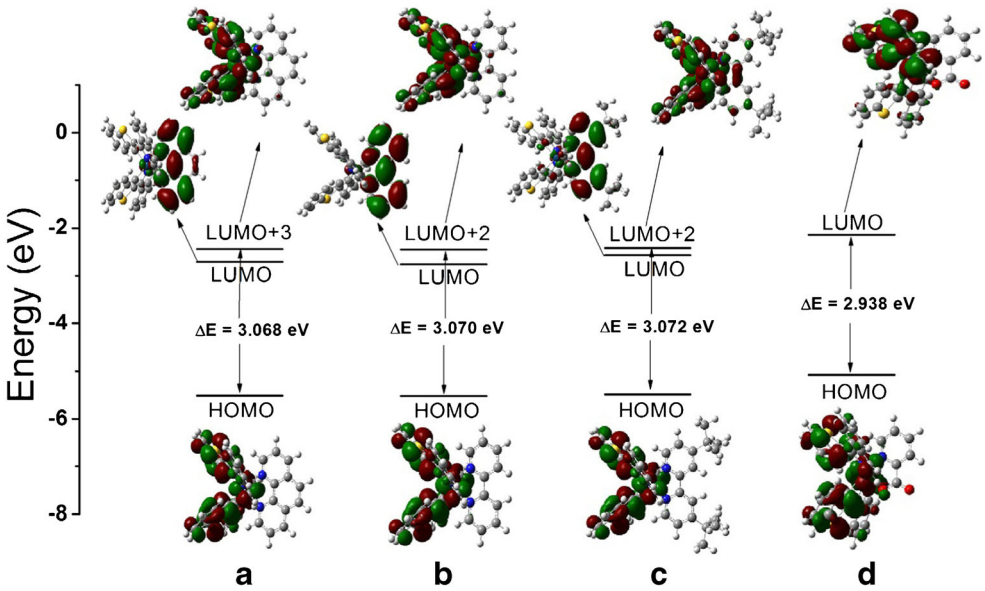

Fig. 3 Molecular orbital energy-level diagrams of complexes 3a−3d

Table 4 Main experimental and calculated optical transitions for complexes 3a−3d

Complex	Orbital excitations	Nature of transition	Oscillation strength	Calcd(nm)	Exptl(nm)
3a	HOMO→LUMO+3	$Ir(d\pi)/L_{btq}(\pi)\rightarrow L_{btq}(\pi^*)$	0.18	501	500
3b	HOMO→LUMO+2	$Ir(d\pi)/L_{btq}(\pi)\rightarrow L_{btq}(\pi^*)$	0.1772	500	490
3c	HOMO→LUMO+2	$Ir(d\pi)/L_{btq}(\pi)\rightarrow L_{btq}(\pi^*)$	0.1709	501	500
3d	HOMO→LUMO	$Ir(d\pi)/L_{btq}(\pi)\rightarrow L_{btq}(\pi^*)$	0.1224	525	525

Table 5 Frontier orbital energy and electron density distribution for complexes 3a−3d

Complex	Orbital	Energy (eV)	Composition (%)			
			Ir	benzothienyl	quinolinyl	Ancillary ligand
3a	LUMO+3	−2.443	6.81	25.13	61.76	6.30
	LUMO	−2.713	3.03	1.26	4.34	91.37
	HOMO	−5.511	22.90	56.00	19.12	1.97
3b	LUMO+2	−2.448	6.86	25.03	64.27	6.37
	LUMO	−2.757	2.68	1.13	4.21	92.03
	HOMO	−5.518	22.96	56.09	19.41	1.94
3c	LUMO+2	−2.415	7.21	23.22	57.43	12.14
	LUMO	−2.569	1.99	2.67	7.97	87.37
	HOMO	−5.487	23.29	55.69	19.03	2.00
3d	LUMO	−2.139	7.11	27.48	62.17	3.25
	HOMO	−5.077	27.31	51.57	18.87	2.25

shown in Fig. 4, the emission spectra of all complexes show broad and structureless, indicating that their emissive excited states have ^{3}MLCT character rather than ligand-centered (^{3}LC) character [39, 40]. From Table 3, it can be seen that the emission maxima are in the range 682–698 nm and their emission colors are deep-red. As for complex 3d, an approximately 16 nm red shift relative to other three complexes 3a−3c is discovered. The fact is also dependent on the nature of ancillary ligand. It is evident from Table 5 that the electron-donating oxygen ion on the pic ligand of complex 3d increases the electron density around the iridium center (27.31 %) and raises the highest occupied molecular orbital (HOMO) level (−5.077 eV), thereby resulting in a distinct HOMO−LUMO energy gap.

Phosphorescence relative quantum yields (Φ) of 3a−3d in dichloromethane solution were measured to be 0.10−0.12

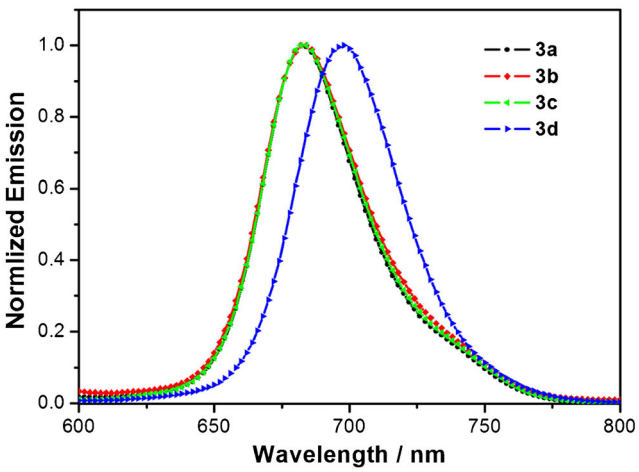

Fig. 4 Normalized emission spectra of complexes 3a−3d in CH_2Cl_2 at room temperature

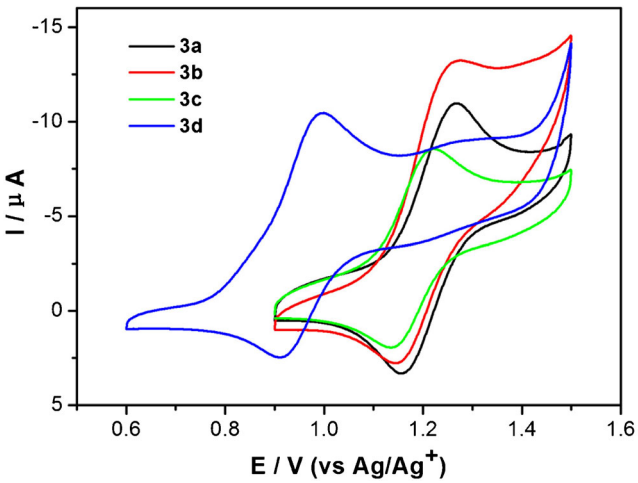

Fig. 5 Cyclic voltammograms of complexes 3a−3d measured in CH_2Cl_2 solution containing n-Bu_4NClO_4 (0.1 M). The scan rate was 100 mV/s

Table 6 Electrochemical data of complexes 3a−3d

Complex	E_{ox} (*V*)	E_{ox}^{onset}(*V*)	HOMO [a] (*eV*)	HOMO [b] (*eV*)
3a	1.27	1.08	−5.88	−5.51
3b	1.27	1.06	−5.86	−5.52
3c	1.22	1.05	−5.85	−5.49
3d	0.99	0.72	−5.52	−5.08

[a] HOMO energies are deduced from the equation HOMO=-(E_{ox}^{onset}+ 4.8eV)

[b] Obtained from theoretical calculations.

(Table 3) at room temperature by using typical phosphorescent *fac*-Ir(ppy)$_3$ as a standard (Φ=0.40). To note, the emission quantum yields of complexes 3c and 3d with electron-donating groups are somewhat higher than that of complex 3b. Additionally, all the luminescent quantum yields are relatively low, which are governed intrinsically by the energy gap law of triplet states. According to extensive investigations of a series of related complexes [9, 41, 42], the luminescence quantum yields of red-emitting iridium(III) phosphors always tend to decrease with an increase in the emission wavelength.

Electrochemical Properties

The electrochemical properties of the complexes 3a−3d were investigated by cyclic voltammetry, and the electrochemical waves are shown in Fig. 5. The HOMO energy levels are also estimated and summarized in Table 6. As depicted in Fig. 5, the complexes 3a−3c show a reversible oxidation peak around 1.22−1.27 V, which is attributed to the oxidation of Ir(III) to Ir(IV) [43]. While the oxidation peak of complex 3d appears at 0.99 V, which is shifted more negative potential than complexes 3a−3c, indicating the destabilization of the HOMO orbital. In order to identify the deduction, the HOMO energy levels for 3a−3d were calculated by the equation HOMO=− (+ 4.8 eV) [44], as well as compared with the theoretical calculation results. From the results, it can be seen that the HOMO orbital energy of complex 3d is higher than complexes 3a−3c. This observation correlates well with the photophysical properties discussed above.

Conclusion

In summary, four new bis-cyclometalated btq-based iridium(III) complexes incorporating different ancillary ligands have been synthesized and fully characterized by FTIR, ^{1}H NMR and mass spectroscopies. The photophysical properties, electrochemical behaviors and theoretical calculations have been investigated. The single crystal X-ray structural studies show that complex 3a adopts a distorted octahedral geometry around the iridium metal exhibiting *cis*-C,C' and *trans*-N,N' chelate disposition. Analyses of DFT and TD−DFT calculations for 3a−3d indicate that the lowest-energy electronic transitions are attributed to ^{1}MLCT transition, and a good agreement with the experimental data is obtained. All Ir(III) complexes exhibit deep-red phosphorescence with similar quantum yields in dichloromethane solution at room temperature. Compared with 3a−3c, the emission spectrum for complex 3d is red-shifted, as a consequence of the nature of the pic ancillary ligand. These research results will facilitate the design of new btq-based ligands for red-emitting iridium complexes.

Acknowledgments This work was supported by the Science and Research Project of Education Department of Hainan Province (No. Hjkj2013-25) and the National Innovation Experiment Program for University Students (The research of metal complexes involving tetrathiafulvalene with triazole and pyridine ligands: syntheses and optoelectronic properties).

References

1. Zhou GJ, Wong WY, Suo S (2010) Progress and current challenges in phosphorescent white organic light-emitting diodes (WOLEDs). J Photochem Photobio C Photochem Rev 11:133–156
2. Kamtekar KT, Monkman AP, Bryce MR (2010) Recent advances in white organic light-emitting materials and devices (WOLEDs). Adv Mater 22:572–582
3. Wu H, Ying L, Yang W, Cao Y (2009) Progress and perspective of polymer white light-emitting devices and materials. Chem Soc Rev 38:3391–3400
4. Wang Q, Ma D (2010) Management of charges and excitons for high-performance white organic light-emitting diodes. Chem Soc Rev 39: 2387–2398
5. D'Andrade BW, Forrest SR (2004) White organic light-emitting devices for solid-state lighting. Adv Mater 16:1585–1595
6. Zhu W, Zhu M, Ke Y, Su L, Yuan M, Cao Y (2004) Synthesis and red electrophosphorescence of a novel cyclometalated iridium complex in polymer light-emitting diodes. Thin Solid Films 446:128–131
7. Tokito S, Iijima T, Tsuzuki T, Sato F (2003) High-efficiency white phosphorescent organic light-emitting devices with greenish-blue and red-emitting layers. Appl Phys Lett 83:2459–2461
8. Lo SC, Namdas EB, Burn PL, Samuel IDW (2003) Synthesis and properties of highly efficient electroluminescent green phosphorescent iridium cored dendrimers. Macromolecules 36:9721–9730
9. Chen CT (2004) Evolution of red organic light-emitting diodes: materials and devices. Chem Mater 16:4389–4400
10. Rodríguez-Redondo JL, Costa RD, Ortí E, Sastre-Santos A, Bolink HJ, Fernández-Lázaro F (2009) Red-light-emitting electrochemical cell using a polypyridyl iridium(III) polymer. Dalton Trans 9787–9793
11. Langdon-Jones EE, Hallett AJ, Routledge JD, Crole DA, Ward BD, Platts JA, Pope SJA (2013) Using substituted cyclometalated quinoxaline ligands to finely tune the luminescence properties of iridium(III) complexes. Inorg Chem 52:448–456
12. Kessler F, Costa RD, Censo DD, Scopelliti R, Ortí E, Bolink HJ, Meier S, Sarfert W, Grätzel M, Nazeeruddin MK, Baranoff E (2012) Near-UV to red-emitting charged bis-cyclometallated iridium(III) complexes for light-emitting electrochemical cells. Dalton Trans 41: 180–191

13. Adachi C, Baldo MA, Forrest SR, Lamansky S, Thompson ME, Kwong RC (2001) High-efficiency red electrophosphorescence devices. Appl Phys Lett 78:1622–1624
14. Kawamura Y, Goushi K, Brooks J, Brown JJ, Sasabe H, Adachi C (2005) 100 % phosphorescence quantum efficiency of Ir(III) complexes in organic semiconductor films. Appl Phys Lett 86:071104-1–071104-3
15. Bae HJ, Chung J, Kim H, Park J, Lee KM, Koh TW, Lee YS, Yoo S, Do Y, Lee MH (2014) Deep Red phosphorescence of cyclometalated iridium complexes by σ-carborane substitution. Inorg Chem 53:128–138
16. Lamansky S, Djurovich P, Murphy D, Abdel-Razzaq F, Lee HE, Adachi C, Burrows PE, Forrest SR, Thompson ME (2001) Highly phosphorescent bis-cyclometalated iridium complexes: synthesis, photophysical characterization, and use in organic light emitting diodes. J Am Chem Soc 123:4304–4312
17. Tsuboyama A, Iwawaki H, Furugori M, Mukaide T, Kamatani J, Igawa S, Moriyama T, Miura S, Takiguchi T, Okada S, Hoshino M, Ueno K (2003) Homoleptic cyclometalated iridium complexes with highly efficient red phosphorescence and application to organic light-emitting diode. J Am Chem Soc 125:12971–12979
18. Ikawa S, Yagi S, Maeda T, Nakazumi H, Fujiwara H, Koseki S, Sakurai Y (2013) Photo- and electroluminescence from deep-red- and near-infrared-phosphorescent tris-cyclometalated iridium(III) complexes bearing largely π-extended ligands. Inorg Chem Commun 38:14–19
19. Juris A, Balzani V, Barigelletti F, Campagna S, Belser P, Vonzelewsky A (1988) Ru(II) polypyridine complexes: photophysics, photochemistry, eletrochemistry, and chemiluminescence. Coord Chem Rev 84:85–277
20. Frank M, Nieger M, Vögtle F, Belser P, Vonzelewsky A, Cola LD, Balzani V, Barigelletti F, Flamigni L (1996) Dinuclear Ru^{II} and/or Os^{II} complexes of bis-bipyridine bridging ligands containing adamantane spacers: synthesis, luminescence properties, intercomponent energy and electron transfer processes. Inorg Chim Acta 242:281–291
21. King KA, Spellane PJ, Watts RJ (1985) Excited-state properties of a triply ortho-metalated iridium(III) complex. J Am Chem Soc 107:1431–143
22. CrysAlisPro Version 1.171.36.21. (2012) Agilent Technologies Inc. Santa Clara, CA, USA
23. Sheldrick GM (2008) A short history of *SHELX*. Acta Cryst Sect A 64:112–122
24. Dolomanov OV, Bourhis LJ, Gildea RJ, Howard JK, Puschmann H (2009) OLEX2: a complete structure solution, refinement and analysis program. J Appl Cryst 42:339–341
25. Frisch MJ, Trucks GW, Schlegel HB, Scuseria GE, Robb MA, Cheeseman JR, Montgomery JA, Vreven T, Kudin KN, Burant JC, Millam JM, Iyengar SS, Tomasi J, Barone V, Mennucci B, Cossi M, Scalmani G, Rega N, Petersson GA, Nakatsuji H, Hada M, Ehara M, Toyota K, Fukuda R, Hasegawa J, Ishida M, Nakajima T, Honda Y, Kitao O, Nakai H, Klene M, Li X, Knox JE, Hratchian HP, Cross JB, Adamo C, Jaramillo J, Gomperts R, Stratmann RE, Yazyev O, Austin AJ, Cammi R, Pomelli C, Ochterski JW, Ayala PY, Morokuma K, Voth GA, Salvador P, Dannenberg JJ, Zakrzewski VG, Dapprich S, Daniels AD, Strain MC, Farkas O, Malick DK, Rabuck AD, Raghavachari K, Foresman JB, Ortiz JV, Cui Q, Baboul AG, Clifford S, Cioslowski J, Stefanov BB, Liu G, Liashenko A, Piskorz P, Komaromi I, Martin RL, Fox DJ, Keith T, Al-Laham MA, Peng CY, Nanayakkara A, Challacombe M, Gill PMW, Johnson B, Chen W, Wong MW, Gonzalez C, Pople JA (2009) Gaussian 09, Revision A.01; Gaussian, Inc.: Wallingford, CT
26. Lee C, Yang W, Parr RG (1988) Development of the colle-salvetti correlation-energy formula into a functional of the electron density. Phys Rev B 37:785–789
27. Miehlich B, Savin A, Stoll H, Preuss H (1989) Results obtained with the correlation energy density functionals of becke and Lee, Yang and Parr. Chem Phys Lett 157:200–206
28. Becke AD (1993) Density-functional thermochemistry. III. The role of exact exchange. J Chem Phys 98:5648–5652
29. Cossi M, Rega N, Scalmani G, Barone V (2003) Energies, structures, and electronic properties of molecules in solution with the C-PCM solvation model. J Comput Chem 24:669–681
30. Tomasi J, Mennucci B, Cammi R (2005) Quantum mechanical continuum solvation models. Chem Rev 105:2999–3094
31. Tsujimoto H, Yagi S, Honda Y, Terao H, Maeda T, Nakazumi H, Sakurai Y (2010) Photoluminescent properties of heteroleptic cyclometalated platinum(II) complexes bearing 1,3-bis(3,4-dibutoxyphenyl)propane-1,3-dionate as an ancillary ligand. J Lumin 130:217–221
32. Lamansky S, Djurovich P, Murphy D, Abdel-Razzaq F, Kwong R, Tsyba I, Bortz M, Mui B, Bau R, Thompson ME (2001) Synthesis and characterization of phosphorescent cyclometalated iridium complexes. Inorg Chem 40:1704–1711
33. Tamayo AB, Alleyne BD, Djurovich PI, Lamansky S, Tsyba I, Ho NN, Bau R, Thompson ME (2003) Synthesis and characterization of facial and meridional tris-cyclometalated iridium(III) complexes. J Am Chem Soc 125:7377–7387
34. Lo KKW, Chung CK, Zhu NY (2003) Synthesis, photophysical and electrochemical properties, and biological labeling studies of cyclometalated iridium(III) bis(pyridylbenzaldehyde) complexes: novel luminescent cross-linkers for biomolecules. Chem Eur J 9:475–483
35. Colombo MG, Brunold TC, Riedener T, Guedel HU, Fortsch M, Buergi HB (1994) Facial tris cyclometalated rhodium(3+) and iridium(3+) complexes: their synthesis, structure, and optical spectroscopic properties. Inorg Chem 33:545–550
36. Serroni S, Juris A, Campagna S, Venturi M, Denti G, Balzani V (1994) Tetranuclear bimetallic complexes of ruthenium, osmium, rhodium, and iridium. synthesis, absorption spectra, luminescence, and electrochemical properties. J Am Chem Soc 116:9086–9091
37. Neve F, Deda ML, Crispini A, Bellusci A, Puntoriero F, Campagna S (2004) Cationic cyclometalated iridium luminophores: photophysical, redox, and structural characterization. Organometallics 23:5856–5863
38. Takizawa SY, Shimada K, Sato Y, Murata S (2014) Controlling the excited state and photosensitizing property of a 2-(2-pyridyl)benzo[b]thiophene-based cationic iridium complex through simple chemical modification. Inorg Chem 53:2983–2995
39. Lu KY, Chou HH, Hsieh CH, Ou Yang YH, Tsai HR, Tsai HY, Hsu LC, Chen CY, Chen IC, Cheng CH (2011) Wide-range color tuning of iridium biscarbene complexes from blue to red by different N∧N ligands: an alternative route for adjusting the emission colors. Adv Mater 23:4933–4937
40. Li H, Yin YM, Cao HT, Sun HZ, Wang L, Shan GG, Zhu DX, Su ZM, Xie WF (2014) Efficient greenish-blue phosphorescent iridium(III) complexes containing carbene and triazole chromophores for organic light-emitting diodes. J Organomet Chem 753:55–62
41. Cummings SD, Eisenberg R (1996) Tuning the excited-state properties of platinum(II) diimine dithiolate complexes. J Am Chem Soc 118:1949–1960
42. Ho CL, Li H, Wong WY (2014) Red to near-infrared organometallic phosphorescent dyes for OLED applications. J Organomet Chem 751:261–285
43. Thomas KR, Velusamy M, Lin JT, Chien CH, Tao YT, Wen YS, Hu YH, Chou PT (2005) Efficient red-emitting cyclometalated iridium(III) complexes containing lepidine-based ligands. Inorg Chem 44:5677–5685
44. Lee W, Kwon TH, Kwon JC, Kim JY, Lee C, Hong JI (2011) Effect of main ligands on organic photovoltaic performance of Ir(III) complexes. New J Chem 35:2557–2563